Subdiffusive motion in kinetically constrained models

Robert L. Jack
Department of Physics, University of Bath, Bath BA2 7AY, United Kingdom
and Department of Chemistry, University of California at Berkeley, Berkeley, California 94720, USA

Peter Sollich
Department of Mathematics, King's College London, London WC2R 2LS, United Kingdom

Peter Mayer
Department of Chemistry, Columbia University, 3000 Broadway, New York, New York 10027, USA
(Received 18 September 2008; published 8 December 2008)

We discuss a kinetically constrained model in which real-valued local densities fluctuate in time, as introduced recently by Bertin, Bouchaud, and Lequeux. We show how the phenomenology of this model can be reproduced by an effective theory of mobility excitations propagating in a disordered environment. Both excitations and probe particles have subdiffusive motion, characterized by different exponents and operating on different time scales. We derive these exponents, showing that they depend continuously on one of the parameters of the model.

DOI: 10.1103/PhysRevE.78.061107 PACS number(s): 05.40.−a, 64.70.qd

I. INTRODUCTION

There has been considerable recent interest in the hypothesis that glassy materials can be described by coarse-grained models with simple thermodynamic properties and nontrivial kinetic constraints [1–8]. These models capture the dynamically heterogeneous nature of glass formers [9]: the implicit assumption is that microscopic details of the glass former are important only insofar as they set the parameters of the coarse-grained dynamical theory. Some kinetically constrained models describe particles hopping on a lattice [10,11]; in other cases, binary (Ising) spins are used [2,12,13], where the two states of the spin represent "mobile" and "immobile" regions of the liquid.

In a recent paper, Bertin, Bouchaud, and Lequeux (BBL) [5] discussed a kinetically constrained model in which molecular degrees of freedom are modeled by a real-valued local density, defined on a lattice. Loosely speaking, regions of high density correspond to immobile sites in the spin description of [12], and regions of low density correspond to mobile sites. However, the continuous range of densities in the BBL model captures the fact that a glass-forming system has a variety of local packings, which may not permit a simple decomposition into mobile and immobile. The continuous range of densities leads to a continuous range of mobilities, resulting in a very broad distribution of relaxation times, characteristic of glassy behavior.

As discussed in Ref. [5], relaxation in the BBL model occurs by means of "mobility excitations" that propagate subdiffusively across the system. Links between broadly distributed relaxation times and subdiffusive motion of particles are quite familiar in theories of glass-forming liquids [14]. Here, we focus initially on the motion of mobility excitations, by coarse-graining the BBL model onto an effective theory for these excitations. This procedure represents a very simple example of the coarse-graining of glassy materials that was proposed by Garrahan and Chandler [2]. The resulting effective theory is a disordered generalisation of the one-spin facilitated Fredrickson-Andersen (FA) model [12]. The possibility of subdiffusive motion in this model is important when comparing model results with experiments on supercooled liquids: on approaching the experimental glass transition time scales increase dramatically, while the length scales associated with dynamical heterogeneity grow more slowly [9,15,16]. In the dynamical facilitation picture [2], the motion of mobility excitations leads to a relation of the form $\tau \sim \xi^z/\Omega$ where z is a dynamical exponent, τ the relaxation time scale, ξ the length scale associated with dynamical heterogeneity, and Ω a (possibly temperature-dependent) constant [17]. Subdiffusion of these excitations corresponds to an exponent $z>2$, consistent with a time scale that increases much more quickly with the corresponding length scale than for ordinary diffusion.

In this paper we focus throughout on the one-dimensional case, where subdiffusion effects are most pronounced [5]. Analysis of the disordered FA model leads us to two main results. First, we are able to explain the scaling exponents observed in [5]. In particular, while the disorder in both the BBL and disordered FA models is fluctuating, we explain why excitations propagate with the scaling laws expected for a particle moving in a quenched random environment. Second, we consider the motion of probe particles in the BBL and disordered FA models. These particles propagate subdiffusively, but with scaling laws that are different from those of the mobility excitations.

The form of the paper is as follows. In Sec. II, we define the BBL model and the disordered FA model. In Sec. III, we use four-point correlation functions [8,18–20] to investigate the subdiffusive propagation of mobility excitations, and we discuss the associated scaling exponents. In Sec. IV, we consider the motion of probe particles in the BBL model, and show that this behavior can also be reproduced in the disordered FA model.

II. MODELS

A. BBL model

The (one-dimensional) BBL model is defined [5] for a chain of continuous densities $\{\rho_i\}$, constrained to $0<\rho_i<2$. Dynamical moves involve rearrangement of the density between adjacent pairs of sites:

$$\rho_i,\rho_{i+1} \to \rho_i',\rho_{i+1}', \quad \text{rate } f_i P_\rho(\rho_i',\rho_{i+1}'|\rho_i+\rho_{i+1}), \tag{1}$$

where $f_i=\Theta(2-\rho_i-\rho_{i+1})$ is the facilitation function for bond i, between sites i and $i+1$. Here, $\Theta(x)$ is the Heaviside step function, so a density rearragement between two sites can occur only if the total density on those sites is less than 2. The distribution of densities after the rearrangement is

$$P_\rho(\rho_i,\rho_{i+1}|R) = A(\rho_i\rho_{i+1})^{\mu-1}\delta(R-\rho_i-\rho_{i+1}), \tag{2}$$

where the δ function enforces volume conservation. The parameter $\mu>0$ was motivated in [5] in terms of an interaction between the particles of the model. If $\mu>1$ then the density after the rearrangment tends to be distributed equally between sites i and $i+1$; if $\mu<1$ then the density is more likely to accumulate on just one of the sites. The coefficient $A=[R^{1-2\mu}\Gamma(2\mu)/\Gamma(\mu)^2]$ is determined by the requirement that

$$\int_0^2 d\rho_i \int_0^2 d\rho_{i+1} P_\rho(\rho_i,\rho_{i+1}|R) = 1, \tag{3}$$

which means that all facilitated bonds rearrange with unit rate. [Here, $\Gamma(\mu)$ is the usual Gamma function.]

These dynamical rules respect detailed balance with respect to a steady state distribution $P_{\text{stat,BBL}}(\{\rho_i\})$ that factorizes between sites. In the grand canonical ensemble we have

$$P_{\text{stat,BBL}}(\{\rho_i\}) = \prod_i P_s(\rho_i), \quad P_s(\rho) \propto \rho^{\mu-1}e^{\gamma\rho}, \tag{4}$$

normalized so that $\int_0^2 d\rho\, P_s(\rho)=1$. Our notation differs from [5] in that we use γ for the Lagrange multiplier conjugate to density, reserving β for the inverse temperature of the FA model.

It is clear from Eq. (1) that motion is possible only across bonds with $f_i=1$. We refer to these as facilitated bonds. The steady state contains a finite fraction of facilitated bonds, which we denote by

$$\eta \equiv \langle f_i \rangle. \tag{5}$$

We also define the mean density,

$$\bar{\rho} \equiv \langle \rho_i \rangle. \tag{6}$$

Facilitated bonds in the BBL model are the fundamental mobility excitations in the system. The interesting scaling limit is the one of maximal mean density $\bar{\rho}\to 2$, where facilitated bonds are rare ($\eta \ll 1$). In this limit, γ is large, and we have

$$\bar{\rho} = 2-\gamma^{-1}+O(\gamma^{-2}), \tag{7}$$

$$\eta = 2\gamma\exp(-2\gamma)\frac{\Gamma(\mu)^2}{\Gamma(2\mu)}[1+O(\gamma^{-1})], \tag{8}$$

consistent with [5]. It was further observed in [5] that the dynamics of these excitations in the BBL model can be represented schematically by the processes

$$01 \leftrightarrow 11 \leftrightarrow 10, \tag{9}$$

where a 1 represents a facilitated bond ($f_i=1$ or $f_{i+1}=1$, respectively), and a 0 an unfacilitated bond ($f_i=0$ or $f_{i+1}=0$). The above two-step process then produces effective diffusion of excitations. When excitations meet, they can coagulate via, e.g., $101\to 111\to 011\to 010$; running through the steps in reverse, a single excitation can also branch into two. Excitations can never be created unless there is already an excitation present on a neighbouring bond, and this is the key motivation for the effective FA models presented below.

When excitations are rare, the rate-limiting step in the effective diffusion is the creation of a new excitation, $01\to 11$. To obtain the typical rate for this process, consider a density rearrangement event across bond $i+1$:

$$\rho_i,\rho_{i+1},\rho_{i+2} \to \rho_i,\rho_{i+1}',\rho_{i+2}'. \tag{10}$$

The process $01\to 11$ occurs when the second bond is facilitated in both initial and final states, while the first bond is facilitated only in the final state. That is,

$$\rho_{i+1}+\rho_{i+2} = \rho_{i+1}'+\rho_{i+2}' < 2,$$

$$\rho_i+\rho_{i+1} > 2,$$

$$\rho_i+\rho_{i+1}' < 2. \tag{11}$$

To work out the typical rate with which these processes occur, we should perform a steady-state average over all initial configurations with the prescribed mobility configuration ($f_i=0$, $f_{i+1}=1$), corresponding to the first two conditions listed. In addition, however, we condition on ρ_i, which strongly influences the rate if it is close to 2: the third condition given above can then only be met if ρ_{i+1}' is very small. Thus, we consider the average rate for the process $(\rho_i=2-\epsilon_i, f_i=0, f_{i+1}=1)\to(\rho_i=2-\epsilon_i, f_i=1, f_{i+1}=1)$, which can only occur via a density rearrangement across bond $i+1$ as written above. The steady-state distribution factorizes between sites and so we have for this rate, denoted by $r_i(\rho_i)$,

$$r_i(\rho_i) = \frac{\displaystyle\int_{\epsilon_i}^2 dR \int_{\epsilon_i}^R d\rho_{i+1} P_s(\rho_{i+1})P_s(R-\rho_{i+1}) \int_0^{\epsilon_i} d\rho_{i+1}' \int_0^2 d\rho_{i+2}' P_\rho(\rho_{i+1}',\rho_{i+2}'|R)}{\displaystyle\int_{\epsilon_i}^2 dR \int_{\epsilon_i}^R d\rho_{i+1} P_s(\rho_{i+1})P_s(R-\rho_{i+1})} \tag{12}$$

where we have introduced $R=\rho_{i+1}+\rho_{i+2}$. The integral over ρ'_{i+2} in the numerator gives $A[\rho'_{i+1}(R-\rho'_{i+1})]^{\mu-1}$, and the one over ρ'_{i+1} then a normalized incomplete Beta function $B(\mu,\mu;\epsilon_i/R)/B(\mu,\mu)$. The remaining average over R (and ρ_{i+1}) becomes concentrated around $R=2$ for large γ, so that in this limit

$$r_i(\epsilon_i)=\frac{B(\mu,\mu;\epsilon_i/2)}{B(\mu,\mu)}=\frac{\int_0^{\epsilon_i/2} dv\, v^{\mu-1}(1-v)^{\mu-1}}{\int_0^1 dv\, v^{\mu-1}(1-v)^{\mu-1}}. \quad (13)$$

Recalling that the local density is $\rho_i=2-\epsilon_i$, we note that dense sites (those with small ϵ_i) lead to small rates r_i.

The relaxation of the BBL model on long time scales is determined by sites with small r_i. For this reason, it is convenient to deduce the distribution of this rate from that of ρ_i, or equivalently ϵ_i. From Eq. (4) one sees for large γ that the variation of the power law factor $\rho^{\mu-1}$ near $\rho=2$ can be neglected, so that $P_s(\epsilon_i)=\gamma\exp(-\gamma\epsilon_i)$. The typical values of ϵ_i are therefore small, $\epsilon_i\sim\gamma^{-1}$, and we can expand the rate as

$$r_i(\rho_i)\simeq a\epsilon_i^{\mu}, \quad a=\frac{\Gamma(2\mu)}{\mu 2^{\mu}\Gamma(\mu)^2}. \quad (14)$$

Transforming then from the distribution of ϵ_i to r_i gives

$$P_{s,r}(r)=\left(P_s(\epsilon_i)\left|\frac{dr_i(\epsilon_i)}{d\epsilon_i}\right|^{-1}\right)_{r=r_i(\epsilon_i)}$$

$$=\frac{1}{\mu\Omega_0}(r/\Omega_0)^{(1/\mu)-1}e^{-(r/\Omega_0)^{1/\mu}}, \quad (15)$$

where

$$\Omega_0=a\gamma^{-\mu}\sim\gamma^{-\mu} \quad (16)$$

is a microscopic rate, which acts as an upper cutoff on the distribution of rates. [The notation $u\sim v$ means that u and v are proportional to each other in the relevant limit (large γ).] It is important to note that the small-r scaling of the distribution $P_{s,r}(r)\sim r^{(1/\mu)-1}$, which we derived above in the limit $\gamma\to\infty$, also applies at finite γ. This is because the rate for small ϵ_i always scales as in Eq. (14), and the probability density $P_s(\epsilon_i)$ of ϵ_i approaches a constant for small ϵ_i for all γ.

The long-time behavior of the BBL model is now controlled by the behavior of $P_{s,r}(r)$ at small r, and, in particular, by the exponent μ. The time for a mobility excitation to diffuse across bond i is of order $1/r_i$. The average diffusion time $\langle 1/r\rangle$, with the average taken over the distribution $P_{s,r}(r)$, then shows a change of behavior at $\mu=1$: for $\mu<1$ it is finite, while for $\mu>1$ it diverges. This motivates why subdiffusion occurs in the second case: for arbitrarily long times t there are a significant number of barriers to mobility diffusion that have transmission rate $<1/t$.

B. Effective FA model

We now describe the effective model that captures the dynamics of the mobile bonds on large length and time scales. In this model, the bonds of the BBL model are represented by a chain of binary variables $\{n_i\}$, where $n_i=1$ if the bond between sites i and $i+1$ of the BBL model is mobile, and $n_i=0$ otherwise. The variable n_i corresponds to the BBL variable f_i. The process of Eq. (9) is then

$$(n_i=0,n_{i+1}=1)\to(n_i=1,n_{i+1}=1). \quad (17)$$

It occurs with a rate $r_i e^{-\beta}$, and the reverse process occurs with rate r_i. Here, $e^{-\beta}$ determines the concentration of sites with $n_i=1$, while r_i is a site-dependent rate whose fluctuations capture the effect of the fluctuating density ρ_i in the BBL model. In our effective model we use the convention $0<r_i<1$; taking a maximal rate of unity sets the unit of time. To mimic the distribution of rates in the BBL model, we define the disordered FA model so that the r_i are distributed independently in the steady state, with

$$P_r(r_i)=(1/\mu)r_i^{(1/\mu)-1}, \quad r_i<1, \quad (18)$$

in accordance with Eq. (15).

The rate r_i in the disordered FA model reflects the local density in the BBL model: it is a fluctuating variable. In the dynamics of the disordered FA model, we account for this fact by randomizing r_i when the process corresponding to Eq. (10) occurs. Hence, we define our disordered FA model by the dynamical rules

$$(n_i,n_{i+1},r_i)\to(n_i,1-n_{i+1},r'_i),$$

$$\text{rate } n_i r_i e^{\beta(n_{i+1}-1)}P_{\text{ann}}(r'_i),$$

$$(n_i,n_{i+1},r_i)\to(1-n_i,n_{i+1},r'_i),$$

$$\text{rate } n_{i+1} r_i e^{\beta(n_i-1)}P_{\text{ann}}(r'_i),$$

where

$$P_{\text{ann}}(r)\propto rP_r(r) \quad (19)$$

{explicitly, $P_{\text{ann}}(r)=[(1/\mu)+1]r^{1/\mu}$}, and the variables $n_i\in\{0,1\}$ and $0<r_i<1$ reside on the sites and bonds of the FA lattice, respectively. We identify this model as a disordered variant of the FA model [12], since the case $P_r(r)=\delta(r-1)$ is the one-spin facilitated one-dimensional FA model. We refer to it as the bond-disordered FA model since the rates r_i are associated with the bonds of the FA lattice.

The "annealed" distribution of rates after randomisation, $P_{\text{ann}}(r'_i)$, is constructed such that the model obeys detailed balance with respect to

$$P_{\text{stat,FA}}(\{n_i\},\{r_i\})\propto\prod_i P_r(r_i)e^{-\beta n_i}. \quad (20)$$

The stationary density of sites with $n_i=1$ is

$$c\equiv\langle n_i\rangle=(1+e^{\beta})^{-1}, \quad (21)$$

which plays the part of the parameter η defined in Eq. (5). The only other parameter in the model is μ, which corresponds directly with μ in the BBL model.

Several other comments are in order. We chose $0<r<1$ above, for convenience. As a result, we do not expect direct correspondence between time units in the original and effec-

tive models [comparing Eqs. (15) and (18), we have effectively set the prefactor Ω_0 to unity]. There is also no exact correspondence between the steady states: in the FA model, there are no spatial correlations at all between the n_i, whereas in the original BBL model neighboring excitations (f_i, f_{i+1}) are correlated via the density variable ρ_{i+1}. Finally, the way rates r_i are linked to the creation and destruction of excitations also does not match exactly. In the original BBL model, we saw above that the process $(f_i=0, f_{i+1}=1) \to (f_i=1, f_{i+1}=1)$ is controlled by the density ρ_i, and is slow when ρ_i is close to 2. Translating to the dual lattice of the FA model, this corresponds to the controlling rate for $(n_i=0, n_{i+1}=1) \to (n_i=1, n_{i+1}=1)$ being associated with the bond between n_{i-1} and n_i, *not* with the bond between n_i and n_{i+1} as we have posited. Thus, e.g., the transient appearance of an excitation, $01 \to 11 \to 01$, randomizes r_i in our FA model but does not change ρ_i in the BBL model so that r_i remains unchanged as well. On the other hand, in an effective diffusion step $01 \to 11 \to 10$ in the BBL model, the second step involves a rearrangement across bond i and so a randomization of ρ_i and hence r_i. This is correctly captured in the FA model, and as effective diffusion is the key process in the dynamics we expect our model to give a qualitatively correct description of the BBL dynamics.

C. Model variants

1. Grand canonical BBL model

The grand canonical expression (4) motivates us to define a modified BBL model in which volume is not conserved. We use the same dynamical rule (1), but replace $P_\rho(\rho_i, \rho_{i+1}|R)$ by

$$P'_\rho(\rho_i, \rho_{i+1}) = A'(\rho_i \rho_{i+1})^{\mu-1} e^{\gamma(\rho_i+\rho_{i+1})} \Theta(2-\rho_i-\rho_{i+1}), \tag{22}$$

where the final state is now independent of the volume in the initial state. These dynamical rules preserve the same equilibrium distribution as that of the original BBL model, as given in Eq. (4). The constant of proportionality A' is set by $\int_0^2 d\rho \int_0^2 d\rho' P'_\rho(\rho, \rho') = 1$ so that bonds rearrange with unit rate, as in the original model.

We will find that propagation of mobile bonds is similar in models with and without conserved density, although the relaxation of density fluctuations will clearly be different.

2. Site-disordered FA models

We also define a site-disordered FA model, in which we associate random rates r_i with the sites of the FA chain, instead of the bonds. The dynamical rules are then

$$(n_i, n_{i+1}, r_i, r_{i+1}) \to (n_i, 1-n_{i+1}, r_i, r'_{i+1}),$$

$$\text{rate } n_i r_{i+1} e^{\beta(n_{i+1}-1)} P_{\text{ann}}(r'_{i+1}),$$

$$(n_i, n_{i+1}, r_i, r_{i+1}) \to (1-n_i, n_{i+1}, r'_i, r_{i+1}),$$

$$\text{rate } n_{i+1} r_i e^{\beta(n_i-1)} P_{\text{ann}}(r'_i).$$

As for the bond-disordered FA model, this model also does not exactly capture how rates are linked to rearrangements in the BBL model; but it does provide for rates to be randomized every time an excitation makes an effective diffusion step, which is the key property for the physics. Indeed, we will see below that the excitations behave similarly for bond and site disorder. However, on introducing probe particles to these disordered FA models, one finds that the site-disordered model provides a better match to the BBL model dynamics. The reasons for this will be explained below.

3. FA models with quenched disorder

Finally, it is convenient to define FA models with quenched disorder, in which the rates r_i do not depend on time. The distribution of rates is simply $P_r(r_i)$ in that case. Interestingly, we will find that quenching the disorder in this way has very little effect on dynamical correlations (after disorder averaging). We note that the quenched bond-disordered FA model has a mapping to a disordered model of appearing and annihilating defects (AA model), and inherits from the latter an exact duality mapping, as in the pure case [21].

III. MOBILITY EXCITATIONS

We now consider the dynamics of the mobility excitations in the BBL model, always in the interesting limit where $\bar{\rho}$ is close to 2. First consider the regime where the parameter μ is small (much less than unity). The BBL model in its steady state then has a bimodal distribution of densities with sharp peaks near zero and 2. In that case, it describes diffusing vacancies in a one-dimensional solid (i.e., high-density background). The disordered FA models, on the other hand, all reduce to the pure FA model in the limit of small μ. All models then exhibit dynamical scaling when the excitation density is small, with exponents

$$(z, \nu) = (2, 1), \quad \mu < 1. \tag{23}$$

Here z is the dynamical exponent that sets the relative scaling of space and time, while the correlation length scales as the average distance between excitations, i.e., $\xi \sim \eta^{-\nu}$ for the BBL model and $\xi \sim c^{-\nu}$ for the FA case.

However, the case of $\mu > 1$ is qualitatively different from that of small μ. For example, the mean time associated with rearrangements is $\langle 1/r \rangle$ which diverges for $\mu > 1$ as explained above [recall Eqs. (15) and (18)]. We therefore expect the disorder to have a strong effect: this is clear from plots of the propensity [22], which we define in terms of the persistence function $p_i(t)$. This function takes a value of unity if the state of site i has not changed between time zero and time t, and $p_i(t)=0$ otherwise. The (time-dependent) propensity for a given initial condition of the system is then $1 - \langle p_i(t) \rangle_{\text{dyn}}$, where the average is over the stochastic dynamics of the system, but with the initial condition fixed [22]. We show sample plots in Fig. 1. In the BBL model, sites with density close to 2 act as barriers to propagation of mobility; in the FA model the same effect arises from bonds with small rates.

A more quantitative measure of the effect of the disorder is its effect on dynamical scaling. It was observed in [5] that the BBL model has scaling exponents close to

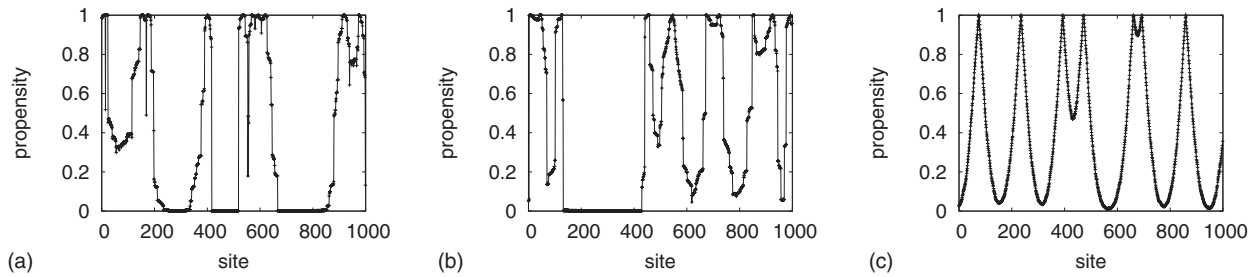

FIG. 1. Typical realizations of the propensity, with times such that the spatially averaged persistence function satisfies $1-\langle p(t)\rangle \simeq 0.4$. Large values of the propensity indicate sites that are very likely to have relaxed, on this time scale. The models with subdiffusive dynamics have large jumps in the propensity, which arise from sites that relax very infrequently. (a) BBL model at $\mu=2$ and $\eta=0.01$. (b) Bond-disordered FA model at $\mu=2$ and $c=0.01$. (c) Pure FA model at $c=0.01$. In the pure case, there are no barriers for excitation propagation, and the propensity is smooth [except near sites with $n_i(t=0)=1$, where it is maximal].

$$(z,\nu) = (1+\mu,1), \quad \mu > 1. \tag{24}$$

An effective model of a single excitation propagating in a quenched environment of random energy barriers gives this scaling, if the distribution of rates for crossing the barriers is $P_r(r)$ [23]. We will discuss below why this quenched result is applicable to the BBL model, which has no quenched disorder. First, though, we show that this subdiffusive scaling can be observed in the four-point functions of both BBL and disordered FA models.

We consider the correlation function

$$G_4(x,t) = \langle \delta p_{i+x}(t)\, \delta p_i(0)\rangle, \tag{25}$$

where $\delta p_i(t) = p_i(t) - \langle p_i(t)\rangle$; $p_i(t)$ is the persistence operator defined above, and the averages are over both initial conditions and the stochastic dynamics. The normalized four point susceptibility is

$$\chi_{4n}(t) \equiv \sum_x G_4(x,t)/G_4(0,t). \tag{26}$$

In one dimension $\chi_{4n}(t)$ is a direct measurement of a growing length scale, when normalized in this way [20,24]. [Note that we evaluate averages in an ensemble with fixed "chemical potential" γ, so that the mean density $\bar{\rho}$ is allowed to fluctuate. Since the dynamics conserve $\bar{\rho}$, this choice does affect the value of $\chi_{4n}(t)$ [8].] In the scaling limit ($\bar{\rho}\to 2$ from below), we expect

$$\chi_{4n}(t) \sim (\Omega t)^{1/z} f(\Omega t/\xi^z) \tag{27}$$

where ξ is the correlation length whose scaling was given above, z is given by Eqs. (23) or (24), as appropriate, Ω is a microscopic rate, and $f(x)$ is a scaling function that is constant at small x and decreases as $x^{-1/z}$ for large x. We argue below that for the BBL model, the rate Ω is equal to Ω_0 [recall Eq. (15)], while for the FA model, we have $\Omega \sim c$ (for small excitation density c).

We show results in Fig. 2. Both models are consistent with Eq. (27); we also find that the FA model exhibits the same scaling as the BBL model, if we identify the excitation densities c and η. Hence we argue that the disordered FA model is an appropriate effective theory for the BBL model.

Figure 2 demonstrates further that BBL models with and without conserved density behave very similarly. We conclude that the conservation of density is not relevant for scaling: this is consistent with the use of the disordered FA model as an effective theory, since that model has no con-

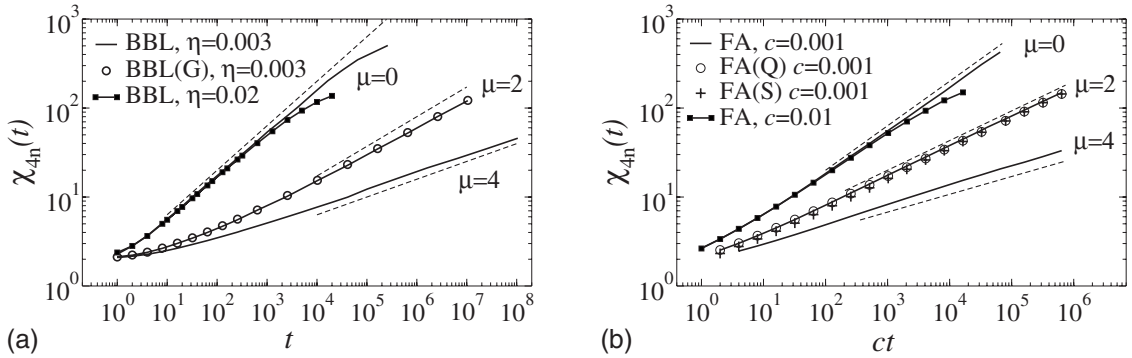

FIG. 2. Subdiffusion in the FA and BBL models is apparent in the four-point susceptibility. (a) We show $\chi_{4n}(t)$ in the BBL model at various μ and η. For the case $\mu=0$, we use a binary distribution of on-site densities $P_s(\rho) \propto \alpha\delta(\rho) + \delta(2-\rho-0^+)$, so that $\eta = \alpha(2+\alpha)/(1+\alpha)^2$; the small offset 0^+ ensures that the facilitation constraint is well defined. The dashed lines show the power law predictions of Eq. (24), and simple diffusive scaling (23) for $\mu=0$. At large times, $\chi_{4n}(t)$ saturates at a value of order η^{-1}: this is apparent in the data for $\mu=0$. The label (G) denotes data for the grand canonical variant of the BBL model. (b) Bond-disordered FA model data with the same values of μ, showing that this effective model captures the four point correlations of the BBL model. The labels (Q) and (S) denote data from the model with quenched bond disorder and fluctuating site disorder respectively; the different variants have very similar behavior.

served density. Quenching the disorder in the FA model has only very weak effects on disorder-averaged properties such as $\chi_{4n}(t)$; finally, differences between bond-disordered and site-disordered models are also very small.

A. Effective barrier models for single excitations

Figure 2 is clear evidence that both BBL and disordered FA models have excitations that propagate subdiffusively at large μ. Further, the dynamical exponents for all the models with $\mu > 1$ seem to satisfy Eq. (24).

For the FA model with quenched bond disorder, this result is to be expected since the motion of independent random walkers in this kind of environment is well understood [23] and does indeed satisfy Eq. (24). However, it was argued in [5] that fluctuating disorder should lead to

$$z = \mu, \quad \mu > 2, \tag{28}$$

and $z=2$ otherwise. This result is inconsistent with the data.

We are not aware of any analysis of fluctuating disorder that is slaved to the motion of the random walker. In this section, we give an argument that explains the applicability of Eq. (24) to the FA model with fluctuating disorder, and hence to the BBL model. While this is not a rigorous proof, the various stages of the argument have been verified by direct simulation.

To describe the motion of a single excitation in a disordered environment, we consider a simple barrier model [23]. A single particle moves on a chain of sites, with independent random hop rates $\{r_i\}$ on the bonds, distributed according to $P_r(r)$. We consider both quenched and fluctuating disorder: if the disorder is fluctuating, then each random rate is redrawn from the distribution $P_{\text{ann}}(r)$ when the bond is traversed by the random walker. We have verified by simulation that both variants of this model do indeed satisfy Eq. (24). We explain this result using an argument related to that of le Doussal, Monthus, and Fisher [25]. The effective dynamics scheme that we use for the barrier model with quenched disorder was described in [26], where it was shown that the effective dynamics are a good description of the quenched barrier model, as long as the exponent μ is large. We give a brief description of the effective dynamics here, referring to [26] for details.

In [25], the authors proposed an effective dynamics for a random walker in a (quenched) one-dimensional energy landscape, made up of "barriers" and "valleys." At each stage of the effective dynamics, the smallest barrier in the system is removed, and the particle moves to the bottom of the valley that contains the origin. The time associated with this process is the inverse transmission rate of the barrier that was removed. For models in which the energy landscape has short-ranged correlations, this effective dynamics mimics the real dynamics of the random walker.

For the quenched barrier model, every site is at zero energy, and sites are separated by barriers of varying heights. The effective dynamics involves successive removal of the smallest barriers. Thus, at a given stage of the dynamics, the remaining barriers divide the system into "effective traps." As discussed in [26], the barrier model requires a modification to the scheme of [25], in that the time at which barrier i is removed depends both on the rate r_i and on the widths of the effective traps to the left and right of barrier i. If the widths of these traps are l_1 and l_2, the time τ_i associated with barrier i is determined by $\tau_i^{-1} = r_i(1/l_1 + 1/l_2)$.

To arrive at the subdiffusive scaling of the quenched barrier model, we assume that, at time t, effective traps have a typical width $\ell(t)$. All barriers with $\tau_i < t$ have been removed; typically, these barriers have $r_i \gtrsim \ell(t)/t$.[1] Thus, the density of remaining barriers is

$$\ell(t)^{-1} \simeq \int_0^{\ell(t)/t} dr\, P_r(r), \tag{29}$$

which yields (for large t)

$$t \sim \ell(t)^{1+\mu}. \tag{30}$$

The root mean square displacement of the diffusing excitation scales with $\ell(t)$, so we identify the dynamic exponent $z = 1 + \mu$, consistent with Eq. (24). As discussed in [26], the effective dynamics scheme is predicated on a separation of time scales between crossing rates for successive barriers. In fact, these time scales become well separated only in the limit of large μ, where the diffusion front of the effective dynamics approaches that of the quenched barrier model. Nevertheless, the effective dynamics turns out to give the correct dynamical scaling (24) of the diffusion front throughout the entire subdiffusive regime, i.e., all the way down to the crossover to simple diffusion at $\mu = 1$.

We now apply this scheme to models with fluctuating disorder. The fluctuations in the disorder have two main effects. First, once large barriers have been crossed, their rates are randomized. Thus, if multiple crossings of the same large barrier are important for the quenched model, we expect different behavior for fluctuating disorder. However, a central assumption of the effective dynamics is that the time to travel a distance ℓ is dominated by the time required for the first crossing of the largest barrier between the initial and final sites [26]. Hence, multiple crossings of large barriers are ignored in the effective dynamics, which should therefore be consistent with fluctuating disorder. The second effect of fluctuating disorder is that barrier transmission rates are being randomized as the excitation moves around, so a barrier which previously had a large transmission rate may acquire a new rate that is very small. This new rate would then act as a high barrier and so have a strong effect on the resulting motion. As before, the time taken to move a distance ℓ will be given by the time taken to cross the largest barrier between initial and final states: this might be a barrier that was present initially, or one that appeared as the excitation moved through the system. The key point here is that the system is in a steady state, so the introduction of new barriers occurs with the same rate as the removal of barriers of the same size. Since barriers are removed only when they are crossed,

[1] As discussed in [26], these arguments based on a typical length scale $\ell(t)$ are valid since the distribution of trap widths l is much narrower than the distribution of time scales τ, so fluctuations in l can be neglected.

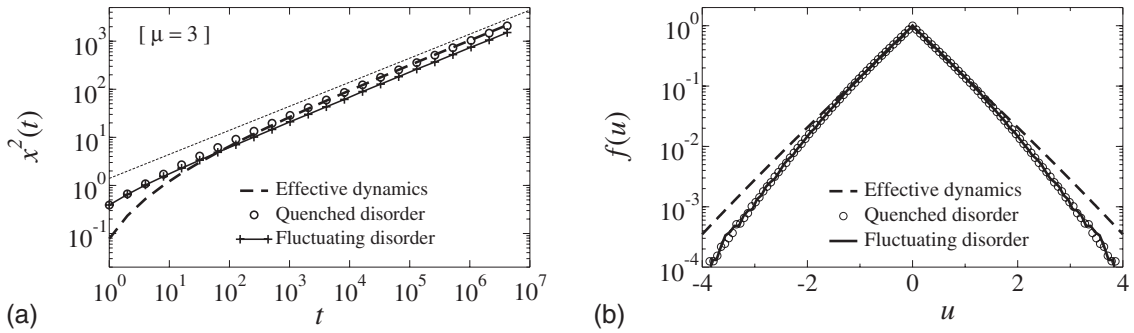

FIG. 3. Dynamics of a random walker in a disordered environment of random energy barriers, where the distribution of barrier-crossing rates is $P_r(r)$, with $\mu=3$. We compare quenched and fluctuating disorder: in the fluctuating case, the rate for hopping between sites i to $i+1$ is randomized whenever the random walker hops between these sites. We compare these two dynamical models with the effective dynamics discussed in the main text. (a) Mean square displacement of the random walker, $x^2(t)$. In the long-time regime, we find dynamical scaling $x^2(t) \simeq (\Omega t)^{2/(1+\mu)} = (\Omega t)^{1/2}$. The power law $x^2 \sim t^{1/2}$ is shown as a light dashed line. The agreement between the effective dynamics and the model with quenched disorder was discussed in [26]. Here we emphasize that the only effect of introducing fluctuating disorder is a small reduction in the prefactor Ω. (b) Scaling form of the diffusion front, normalized to equal height at the origin. That is, we write the distribution of the particle displacement as $P(x|t) = P(0|t) f[xP(0|t)]$ and we plot the function $f(u)$. Within the scaling regime, $f(u)$ does not depend on the time t: the data shown were obtained at $t=2^{22}$, for which this condition is satisfied. The results for models with quenched and fluctuating disorder are very similar. As discussed in [26], deviations between the models and the effective dynamics are expected for finite μ, but vanish in the limit of large μ.

barriers that appear in the system are typically of a size comparable with those that have already been crossed at least once. In the language of the effective dynamics, these barriers are "irrelevant." For these reasons, the effective dynamics apply equally well to models with quenched and fluctuating disorder, and we expect the dynamical exponent $z=1+\mu$ for both cases. This expectation is verified in Fig. 3. We emphasise that while the effective dynamics gives accurate predictions for the diffusion front only when μ is large [26], it gives the correct dynamical scaling for all $\mu>1$: we show this by presenting data for the relatively modest value of $\mu=3$.

Of course, the situation would be very different if the fluctuating disorder was annealed in a two-sided way, where every time an excitation moved to a new site one randomizes the rates for both of the barriers adjacent to that site. This would produce a continuous-time random walk [23], with subdiffusion exponents as in Eq. (28).

To obtain the scaling of length and time scales in the FA and BBL models, we note that the equilibrium spacing between defects sets the dynamical correlation length ξ (for these one-dimensional models). We define the persistence time τ_p by $\langle p_i(\tau_p)\rangle = 1/e$, where $p_i(t)$ is the persistence function, defined above. As in the pure FA model, τ_p scales with the time taken for an excitation to propagate a distance ξ, so we identify $\tau_p \sim \Omega^{-1}\xi^z$, consistent with Eq. (27). To obtain the scaling of Ω with the excitation density η or c, it is useful to rephrase the scaling argument associated with the effective dynamics. In the BBL model, Eq. (15) implies that the fraction of sites with rate $r_i < r$ scales as

$$n(r) \sim (r/\Omega_0)^{1/\mu} \tag{31}$$

for small r. Thus, moving a distance ℓ typically requires the particle to cross a barrier whose transmission rate is $r_i \simeq \Omega_0 \ell^{-\mu}$. The time taken to cross such a barrier is typically $\tau_i \sim \ell / r_i \sim \Omega_0^{-1} \ell^{1+\mu}$. This is consistent with Eq. (30), and it allows us to identify the coefficient Ω in Eq. (27) with Ω_0 in Eq. (15). In the FA model, crossing a barrier with transmission rate r_i typically requires a spin to flip from state 0 to state 1, and this process occurs with rate $e^{-\beta} \sim c$. Thus, moving a distance ℓ typically requires the crossing of a barrier with $r_i \simeq \ell^{-\mu}$, which takes a time $\tau_i \sim \ell/(r_i c) \sim c^{-1}\ell^{1+\mu}$. Thus, we identify the coefficient Ω in Eq. (27) with the inverse excitation density c. Overall, for $\mu>1$, we arrive at $\tau_p \sim c^{-2-\mu}$ for the FA model, and $\tau_p \sim [\ln(1/\eta)]^{-\mu} \eta^{-1-\mu}$ for the BBL model, where we used $\Omega_0 \sim \gamma^{-\mu} \sim [\ln(1/\eta)]^{-\mu}$.

We conclude that the effective dynamics scheme presented here captures the propagation of mobility excitations in the BBL and disordered FA models on large length and time scales, even though the BBL model has nontrivial dynamical correlations in the densities ρ_i which the coarse-grained FA model neglects. This analysis demonstrates that the scaling properties of the persistence time and the four-point susceptibility, as expressed in Eqs. (23), (24), and (27), can be understood in terms of independently propagating (noncooperative) excitations.

B. Long-time limit

So far, we have considered time scales up to the persistence time τ_p: excitations move distances smaller than their typical spacing, and can be treated independently. We now turn to much longer time scales. The assumption of independently propagating defects in one dimension leads to a persistence function consistent with the results of [5]:

$$p(t) \equiv \langle p_i(t)\rangle = \exp\left(-\frac{(\Omega t)^{1/z}}{\xi}\right) \tag{32}$$

for $t \gg 1$.

However, for times larger than τ_p, this prediction fails. For example, in the site-disordered FA model, the fraction of

sites with rate $r_i < r$ is $n(r) = r^{1/\mu}$. At infinite temperature ($\beta = 0, c = 1/2$), the facilitation constraint in the FA model can be ignored (most sites are faciliated). In that case, the typical time taken to flip (for the first time) a site with initial rate r_i is $\tau_i = 1/r_i$. Thus, the persistence function decays as $\langle p_i(t)\rangle_{\beta=0} \simeq n(t^{-1}) \simeq t^{-1/\mu}$. Lowering the temperature in the FA model only slows down the dynamics, so $\langle p_i(t)\rangle \gtrsim t^{-1/\mu}$ for all times and temperatures. Thus, Eq. (32) must break down at long times: we attribute this breakdown to the fact that a single site with a small rate r_i can block the motion of several excitations.

We now consider this long-time regime in more detail, and return to the effective dynamics picture, working with a finite density of excitations, η. If the density of relevant barriers is larger than the density of excitations, each effective trap typically contains at most one excitation, and excitations can be treated independently. However, when the spacing between relevant barriers becomes larger than the distance between excitations, one enters a different regime. To see this, note that the typical time scale associated with rearrangement of a "slow" (relevant) site i in the BBL model is generically $\tau_i = 1/[r_i(\eta_{i-1} + \eta_{i+1})]$ where η_{i-1} and η_{i+1} are the excitation densities in the effective traps to left and right of site i. (Recall that r_i is the rate with which the relevant site rearranges, given that there is an excitation adjacent to that site. Thus, the time taken to flip a relevant site depends on the density of excitations in the adjacent traps.)

In the short-time regime where there are many more effective traps than there are excitations, then we can write $\eta_i \simeq 1/l_i$ if trap i contains an excitation, and $\eta_i = 0$ otherwise (as above, l_i is the width of the effective trap i). Considering a site i for which one of the adjacent traps contains an excitation, we arrive at the scaling relation $\tau_i \simeq l_i/r_i \simeq \ell/r_i$, as discussed above. However, if there are more excitations than effective traps, we expect the density in each trap to be close to its equilibrium value $\eta_i \simeq \eta_{i+1} \simeq \eta$. Thus, we expect $\tau_i \sim (2\eta r_i)^{-1}$ for $\ell\eta \gg 1$. In both cases, for a given time t, we use $n(r) \simeq (r/\Omega)^{1/\mu}$ to evaluate the fraction of sites with $\tau_i < t$: the mean spacing between these "relevant" sites is $\ell(t)$. The result is

$$\ell(t) \sim \begin{cases} (\Omega t)^{1/(1+\mu)}, & \ell(t) \ll \xi, \\ (\Omega t/\xi)^{1/\mu}, & \ell(t) \gg \xi, \end{cases} \tag{33}$$

where we have used $\xi \sim \eta^{-1}$. For long times, the exponent $1/\mu$ sets the time dependence of $\ell(t)$: this result applies for all $\mu > 0$. In the short-time regime, Eq. (33) is consistent with the analysis of the previous section, and with Eq. (27), as long as $\mu > 1$. However, if $\mu < 1$, the motion of excitations is diffusive: thus, in the short-time regime, there is no distinction between relevant and irrelevant barriers. This means that if $\mu < 1$, the spacing between relevant barriers, $\ell(t)$, is only well defined in the long-time limit, and the short-time scaling regime of Eq. (33) does not exist.

We observe that in the long time limit, $\ell(t)$ represents the mean spacing between isolated sites with small rates r_i, and these sites dominate the long-time limit of the persistence function. That is, in the long-time scaling regime, Eq. (32) is replaced by

$$p(t) \simeq \ell(t)^{-1} \simeq (\Omega t/\xi)^{-1/\mu}. \tag{34}$$

The crossover between the two scaling regimes occurs when $\ell(t) \simeq \xi \simeq \eta^{-1}$ or c^{-1}, respectively. This can be observed in the long-time behavior of the persistence function in the site-disordered FA model. To obtain the long-time limit of this function more quantitatively, we decompose the persistence $p(t) = cp_1(t) + (1-c)p_0(t)$ into contributions from sites that were initially in states 1 and 0 [these two populations have weights c and $(1-c)$, respectively]. Then, in the long-time regime $\ell \gg \xi$, we have $\tau_i \simeq (2cr_i)^{-1}$ for sites that were initially in state 1, given that each of the two facilitating neighbour sites contains a defect with probability c. For those sites initially in state 0, the spin flip rate is suppressed by $e^{-\beta}$, leading to $\tau_i \simeq (2ce^{-\beta}r_i)^{-1}$. The persistence functions are then estimated as the density of sites with $\tau_i > t$, giving $p_1(t) = n(1/(2ct))$ and $p_0(t) = n(1/(2ce^{-\beta}t))$, respectively. Using $n(r) = r^{1/\mu}$, we thus arrive at

$$p(t) \simeq (\lambda t)^{-1/\mu}, \quad \ell(t) \gg \xi \sim c^{-1}, \tag{35}$$

with

$$\lambda = 2ce^{-\beta}[1 + c(e^{-\beta/\mu} - 1)]^{-\mu}. \tag{36}$$

In the limit of dilute excitations ($c \ll 1$) this reduces to $\lambda \sim c^2$. Identifying $p(t)$ with $\ell(t)^{-1}$, this result is consistent with Eq. (33), since we argued in Sec. III A that $\Omega \sim c$ for the FA model.

Results are shown in Fig. 4: at infinite temperature the power law behavior of the persistence is clear. At lower temperatures, the crossover to power law behavior occurs deep in the tails of the persistence [$p(t) \lesssim c$]. In the FA model, this long-time regime can be demonstrated by simulations at high temperature, on relatively short time scales. However, in the BBL model, the equivalent of the high-temperature regime requires small γ, increasing the prefactor Ω_0, and reducing the fraction of sites with small r_i. This means that very long simulations are required to access the long-time limit in the BBL model, and we do not show numerical data in this case. However, the simulations of the site-disordered FA model confirm the validity of the arguments of this section, which apply to both FA and BBL models. (To observe the long-time regime in the bond-disordered FA model, one would need to define and measure a persistence observable on bond i, associated with the rearrangement of density across that bond.)

IV. PROBE PARTICLES

It is a familiar feature of kinetically constrained models that propagation of probe particles is different from that of excitations [3,4,6,27]. We now turn to probe particle motion in the BBL and disordered FA models.

A. Probes in the BBL model

We introduce (noninteracting) probe particles to the BBL model as follows. A probe can move along a bond when density rearranges across that bond. If the bond connects sites i and $i+1$, then after the rearrangement, the probe occupies site i with probability $\rho_i/(\rho_i + \rho_{i+1})$. The joint station-

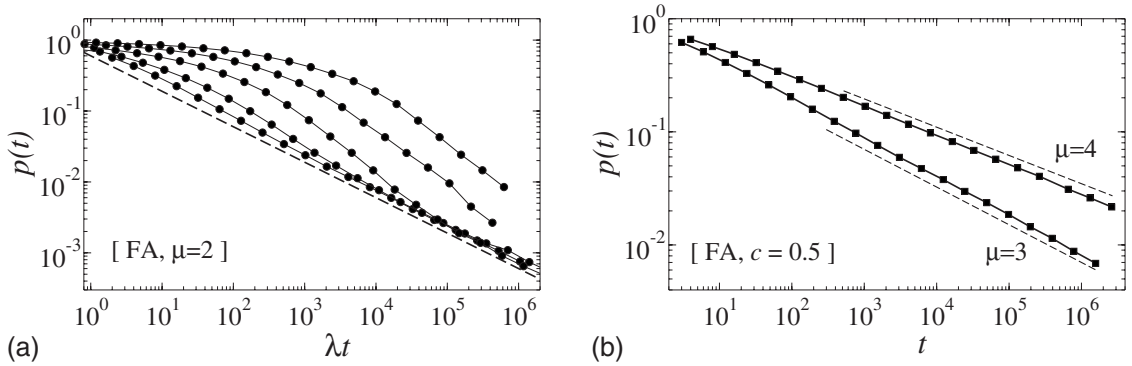

FIG. 4. (a) Persistence function, plotted against the scaling variable λt in the site-disordered FA model. We show data for $c=0.5$, 0.27, 0.12, 0.047, 0.018 (decreasing from left to right; these are inverse temperatures $\beta=0$, 1, 2, 3, 4). As discussed in the text, the persistence time scales as $\tau_p \sim c^{-2-\mu} \sim c^{-4}$, but we use the variable variable λt to verify the long time prediction of Eq. (35): the dashed line shows a power law with exponent 1/2. (b) Persistence at infinite temperature and varying μ. Again, dashed lines show power laws with exponents predicted by Eq. (35).

ary distribution for the probe position and the BBL densities is

$$P_{\text{probe,stat}}(X,\{\rho_i\}) \propto \rho_{i=X} \prod_i P_s(\rho_i), \tag{37}$$

where X is the position (site index) of the probe. Thus, the probability of finding a probe on site $i=X$ is proportional to the local BBL density on that site, $\rho_{i=X}$. This is consistent with the probe representing a typical particle in the BBL model, before the coarse-graining into the densities ρ_i is carried out. An alternative rule, which is more consistent with the effective FA model described below, is to assign the probe with equal probability to sites i and $i+1$. As we discuss below, the excitation motion in these models sets bounds on the motion of the probes: we are primarily concerned with the situation in which these bounds are saturated, in which case details of the microscopic probe motion should be irrelevant. When the bounds are not saturated, the choice of dynamical rule does produce quantitative differences, although qualitative features are preserved.

B. Probes in the FA model

We couple probe particles to the FA model using the method of [3]. Probes can hop between pairs of adjacent sites only when both sites have $n=1$; they attempt these hops with unit rate. With these rules, the equilibrium distribution analogous to Eq. (37) is independent of X: that is, the distribution of the probe position decouples from the excitation variables n_i and the rates r_i.

From the data presented above on the excitation dynamics of the site-disordered and bond-disordered FA models, one might expect that the two model variants also exhibit similar probe dynamics. However, this is not the case because barriers to excitation diffusion act differently on the probes. To see this, consider the site-disordered model, and suppose that site i starts with $n_i=0$ and with a small rate r_i. The probe cannot cross this site until its excitation state changes to $n_i=1$. The rate for this is of order cr_i, and so the rate for a probe to cross this site also vanishes with r_i: high barriers for excitations (small r_i) are also high barriers for probes in the site-disordered FA model.

Now consider the bond-disordered FA model, focusing on a particular bond i, with a small rate r_i. The probe particle can cross this bond if $n_i=1$ and $n_{i+1}=1$: this state can occur on time scales much shorter than $(cr_i)^{-1}$ if an excitation arriving from the right facilitates n_{i+1} and another excitation arriving from the left facilitates n_i. This process sets a rate for crossing the slow bond that is independent of r_i. So the barriers for excitation diffusion have a much smaller effect on probe propagation in the bond-disordered model. (One way to avoid this behavior would be to allow the probe to move along bond i only when the rate for that bond is randomized, but we have not pursued this as we wanted to keep the probe dynamics similar to that used in [3].)

It is clear that in the original BBL model, the barriers for excitation diffusion do also act on probes. A high barrier here is a site with density $\rho_i \approx 2$. This can take part in a rearrangement only once a rearrangement of neighbouring sites has produced a low-density $\rho_{i-1} < 2-\rho_i$ or $\rho_{i+1} < 2-\rho_i$. The rate for these processes, and hence for probe diffusion across site i, vanishes as $\rho_i \to 2$. In summary, only the site-disordered FA model can provide an accurate representation of the BBL probe dynamics because it retains the effect of high barriers on the probes. We therefore do not consider the bond-disordered case in the following.

C. Results for probe motion

In the BBL and site-disordered FA models, the preceding discussion illustrates that sites with small rate r_i are able to block the propagation of probes. Taking the FA model for concreteness, the probe cannot pass any site for which $n_i=0$ for all times between 0 and t. As discussed in Sec. III B, the mean spacing between these sites scales as $t^{1/\mu}$ for large times t. This sets a limit on probe motion,

$$\langle X(t)^2 \rangle \lesssim \ell(t)^2 \sim t^{2/\mu}. \tag{38}$$

For $\mu<2$, this bound is irrelevant: the probes simply diffuse. However, for $\mu>2$, we expect this bound to be saturated at

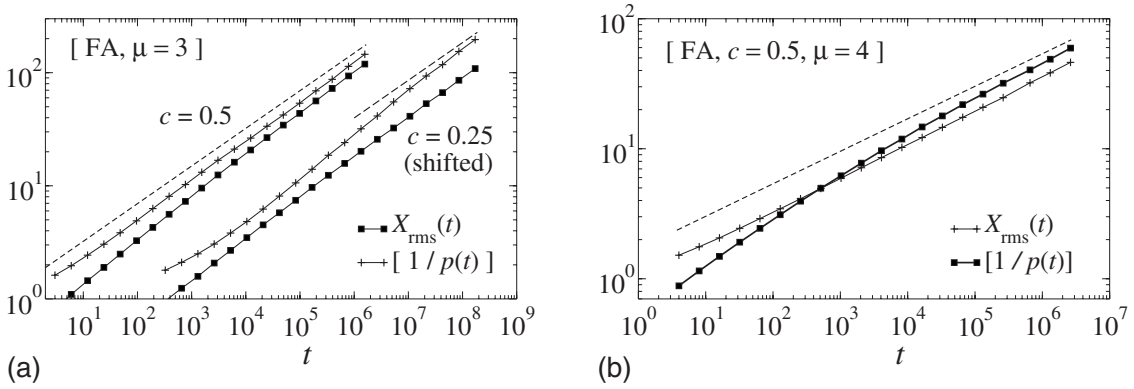

FIG. 5. Comparison of root mean square probe displacement $X_{\rm rms}(t)=\langle X(t)^2\rangle^{1/2}$ with the inverse of the persistence function $1/p(t)$, for the site-disordered FA model. We show data at $\mu=3$ (a) and 4 (b). We have offset the data at $c=0.25$ for clarity: the ordinate is $10t$ in that case. In the long-time limit, the persistence scales as $t^{-1/\mu}$ (this power law is illustrated with dashed lines). At long times the persistence sets a bound on the scaling of the mean square displacement, which appears to saturate for long times.

large times. At long times, we have $\ell(t)\sim p(t)^{-1}$ [recall Eq. (34)]. Thus, Fig. 5 demonstrates that the bound (38) does saturate at long times, although we note that the times required are quite large, even at infinite temperature ($c=1/2$). Physically, the length scale $\ell(t)$ represents the size of an effective trap: saturation of the bound requires that the probe particle explores the whole of the trap before the barriers delimiting the trap become irrelevant. The scaling arguments presented here do not allow us to estimate the time required to reach this regime. However, Eq. (38) shows that probe propagation must be asympotically subdiffusive for all $\mu>2$, and the data are consistent with saturation of this bound throughout this regime.

We emphasize that, while Fig. 5 demonstrates that Eq. (38) holds on long time scales in the FA model, the scaling arguments presented here apply equally well to the BBL model, so asymptotic probe motion in that model must be subdiffusive for $\mu>2$.

We now turn to time scales shorter than τ_p, for which the length scale ℓ again sets a bound on probe motion. Following [4], we decompose the probes into two populations: those that have moved at least once, and those which have not moved at all. We denote the fraction of probes that have moved at least once by $\pi(t)$. Confinement of probes by sites that are persistently unfacilitated again sets an upper bound on the displacement of probes:

$$\frac{\langle|X(t)|^n\rangle}{1-\pi(t)} \lesssim \ell(t)^n, \tag{39}$$

where the left-hand side is the nth moment of the distance moved by those probes that have moved at least once, and the scaling of $\ell(t)$ was given in Eq. (33). Again, saturation of this bound occurs when motion of the probe particle within the effective trap is fast enough that the probe can delocalize within the trap before the barriers delimiting the trap become irrelevant. In the joint limit of large time and large μ, the time scales associated with adjacent barriers become well separated [25,26], allowing equilibration to take place. Thus, for large μ, we expect the bound of Eq. (39) to be saturated for times $t\gg 1$, even if $t\ll\tau_p$.

Assuming saturation of the bound Eq. (39) and $t\ll\tau_p$, the probe persistence scales as $1-\pi(t)\sim 1-\exp[-\ell(t)/\xi]\sim\ell(t)/\xi$. [This is the same scaling as for the excitation persistence in Eq. (32).] Combining this with Eq. (33), we arrive at

$$\langle|X(t)|^n\rangle \sim \xi^{-1}(\Omega t)^{(1+n)/(1+\mu)}. \tag{40}$$

Our simulations are restricted to finite time scales and values of μ that are not very large, so we are not able to investigate this bound in detail. However, the results shown in Fig. 6 are certainly consistent with the prediction of Eq. (40).

V. CONCLUSION

To summarize our main results, we have established that probes and mobility excitations both propagate subdiffusively in the BBL model, and that this subdiffusive behavior can be reproduced in a simple effective FA model. This observation allows us to analyze the subdiffusive motion, and to predict the dynamical exponents for both excitations and probes in the subdiffusive regime [Eqs. (24) and (38)]. A key part of the reasoning consists in showing that quenched and annealed disorder lead to qualitatively the same behavior. This allowed us to deduce that correlation length and time scales are related in these models, by $\tau\sim\xi^{1+\mu}$. When μ is large, we conclude that the very broad distribution of rates in these models leads to a relaxation time that increases much more quickly than the associated length scales, on approaching the glass transition.

We also identify two kinds of subdiffusive motion in these models. On time scales $1\ll t\ll\tau_p$, mobility excitations propagate independently and subdiffusively, according to

$$\langle X^2\rangle \simeq (\Omega t)^{2/(1+\mu)}. \tag{41}$$

The mean square displacement for probes is different and given by Eq. (40) with $n=2$. One has to remember though that the associated root mean square displacement $\langle X^2\rangle^{1/2}$ does not define a length scale for probe motion, since it arises from an average over a dominant population of probes that have not yet moved, and a smaller population that has

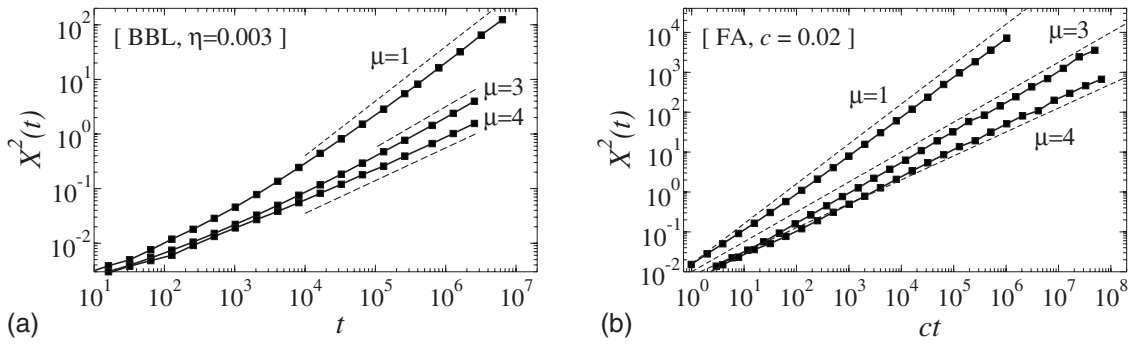

FIG. 6. Mean square probe displacements in the BBL and FA models, for times shorter than τ_p. (a) BBL model. For $\mu>2$, the dashed lines show the predictions of Eq. (40); for $\mu=1$, we show a diffusive law $\langle X^2(t)\rangle \sim t$. (b) Site-disordered FA model, with the same power law predictions. In both cases, we expect a crossover at long times to the asymptotic scaling of Eq. (38).

moved by $(\Omega t)^{1/(1+\mu)}$. For the same reason the exponent for the scaling of $\langle |X(t)|^n \rangle$ in Eq. (40) is not simply proportional to n. On time scales $t \gg \tau_p$, excitations coagulate and branch, and it is not consistent to discuss motion of a single excitation. However, in this long-time regime, probe particles propagate subdiffusively, according to

$$\langle X^2 \rangle \simeq (\Omega t/\xi)^{2/\mu}. \tag{42}$$

The presence of different dynamical exponents for probes and excitations may seem surprising, but we emphasize that Eqs. (41) and (42) apply in separate scaling regimes. (When the concentration of excitations is small, the persistence time $\tau_p \gg 1$ separates two well-defined scaling regimes; of course t is always taken to be large compared to unity.)

Conceptually, it is interesting to note that, in the pure FA model at low temperature, relaxation is controlled by rare active sites (defects). In the disordered model, on the other hand, rare inactive regions (sites with small r_i) play at least as important a role.

Finally, our results for probe particles imply that the Stokes-Einstein relation [9] between relaxation time and probe diffusion constant, $D\tau \sim 1$, has broken down completely in these systems. In the pure FA model, $D\tau$ diverges at low temperatures [3]. On the other hand, in the disordered model, the presence of sites (or barriers) with arbitrarily small rate r_i means that the persistence decays as a power law for large times, while the motion of the probes is subdiffusive even in the long-time limit. However, we can define an analog of the Fickian length $\ell_F = \langle X^2(\tau_p)\rangle^{1/2}$ which represents the distance traveled by a probe, through repeated encounters with a single excitation [4]. If the bound of Eq. (39) is saturated we arrive at $\ell_F \simeq \ell(\tau_p) \simeq \xi$. For the site-disordered FA model, this leads to $\ell_F \sim c^{-1}$, at least for large μ; on the other hand, in the pure FA model, $\ell_F \sim c^{-1/2}$. Physically, confinement of the excitation in an effective trap means that it facilitates any probes in that trap very many times, allowing the probe to delocalize thoughout the trap. In this way, the presence of large barriers to excitation diffusion in the BBL and disordered FA models strengthens the effects discussed in [3,4], in which the square of the Fickian length represents the number of hops that a probe makes through multiple encounters with a single excitation.

ACKNOWLEDGMENTS

We thank L. Berthier, J.-P. Bouchaud, D. Chandler, and J. P. Garrahan for discussions. While at Berkeley, R.L.J. was funded initially by NSF Grant No CHE-0543158 and later by the Office of Naval Research Grant No. N00014-07-1-0689.

[1] For a review, see F. Ritort and P. Sollich, Adv. Phys. **52**, 219 (2003).
[2] J. P. Garrahan and D. Chandler, Phys. Rev. Lett. **89**, 035704 (2002).
[3] Y.-J. Jung, J. P. Garrahan, and D. Chandler, Phys. Rev. E **69**, 061205 (2004).
[4] L. Berthier, D. Chandler, and J. P. Garrahan, Europhys. Lett. **69**, 320 (2005).
[5] E. Bertin, J.-P. Bouchaud, and F. Lequeux, Phys. Rev. Lett. **95**, 015702 (2005).
[6] D. Chandler, J. P. Garrahan, R. L. Jack, L. Maibaum, and A. C. Pan, Phys. Rev. E **74**, 051501 (2006).
[7] C. Toninelli, G. Biroli, and D. S. Fisher, Phys. Rev. Lett. **96**, 035702 (2006).
[8] L. Berthier *et al.*, J. Chem. Phys. **126**, 184504 (2007).
[9] For reviews of the effects of dynamical heterogeneity and breakdown of the Stokes-Einstein relation, see H. Sillescu, J. Non-Cryst. Solids **243**, 81 (1999); M. D. Ediger, Annu. Rev. Phys. Chem. **51**, 99 (2000), S. C. Glotzer, J. Non-Cryst. Solids **274**, 342 (2000); R. Richert, J. Phys.: Condens. Matter **14**, R703 (2002); H. C. Andersen, Proc. Natl. Acad. Sci. U.S.A. **102**, 6686 (2005).
[10] W. Kob and H. C. Andersen, Phys. Rev. E **48**, 4364 (1993); C. Toninelli, G. Biroli, and D. S. Fisher, J. Stat. Phys. **120**, 167 (2005); C. Toninelli, G. Biroli, and D. S. Fisher, Phys. Rev. Lett. **96**, 035702 (2006).
[11] J. Jäckle and A. Krönig, J. Phys.: Condens. Matter **6**, 7633 (1994); A. C. Pan, J. P. Garrahan, and D. Chandler, Phys. Rev.

E **72**, 041106 (2005).
[12] G. H. Fredrickson and H. C. Andersen, Phys. Rev. Lett. **53**, 1244 (1984).
[13] S. Eisinger and J. Jäckle, J. Stat. Phys. **73**, 643 (1993).
[14] T. Odagaki and Y. Hiwatari, Phys. Rev. A **41**, 929 (1990); C. Monthus and J.-P. Bouchaud, J. Phys. A **29**, 3873 (1996).
[15] X. H. Qiu and M. D. Ediger, J. Phys. Chem. B **107**, 459 (2003).
[16] C. Dalle-Ferrier, C. Thibierge, C. Albo-Simionesco, L. Berthier, G. Biroli, J.-P. Bouchaud, F. Ladieu, D. L'Hote, and G. Tarjus, Phys. Rev. E **76**, 041510 (2007).
[17] S. Whitelam, L. Berthier, and J. P. Garrahan, Phys. Rev. Lett. **92**, 185705 (2004).
[18] S. Franz, C. Donati, G. Parisi, and S. C. Glotzer, Philos. Mag. B **79**, 1827 (1999).
[19] L. Berthier, Phys. Rev. E **69**, 020201(R) (2004).
[20] C. Toninelli, M. Wyart, L. Berthier, G. Biroli, and J.-P. Bouchaud, Phys. Rev. E **71**, 041505 (2005).
[21] R. L. Jack, P. Mayer, and P. Sollich, J. Stat. Mech.: Theory Exp. (2006) P03006.
[22] See, for example, A. Widmer-Cooper, P. Harrowell, and H. Fynewever, Phys. Rev. Lett. **93**, 135701 (2004); A. Widmer-Cooper and P. Harrowell, J. Chem. Phys. **126**, 154503 (2007).
[23] J.-P. Bouchaud and A. Georges, Phys. Rep. **195**, 127 (1990).
[24] R. L. Jack, L. Berthier, and J. P. Garrahan, Phys. Rev. E **72**, 016103 (2005).
[25] P. Le Doussal, C. Monthus, and D. S. Fisher, Phys. Rev. E **59**, 4795 (1999).
[26] R. L. Jack and P. Sollich, J. Phys. A **41**, 324001 (2008).
[27] R. L. Jack, D. Kelsey, J. P. Garrahan and D. Chandler, Phys. Rev. E **78**, 011506 (2008).